The Astrophysical Journal, 821:14 (10pp), 2016 April 10 doi:10.3847/0004-637X/821/1/14

CONSTRAINING THE ANGULAR MOMENTUM EVOLUTION OF V455 ANDROMEDAE

Anjum S. Mukadam[1,2], Stylianos Pyrzas[3], D. M. Townsley[4], B. T. Gänsicke[5], J. J. Hermes[6,10], Paula Szkody[1,2], Jonathan Kemp[7], J. Patterson[8], Claire Ding[8], Katie Wolf[8], Marina Gemma[8], Emir Karamehmetoglu[8], and John Rock[9]
[1] Department of Astronomy, University of Washington, Seattle, WA 98195-1580, USA
[2] Apache Point Observatory, 2001 Apache Point Road, Sunspot, NM 88349-0059, USA
[3] Qatar Environment and Energy Research Institute (QEERI), HBKU, Qatar Foundation, P.O. Box 5825, Doha, Qatar
[4] Department of Physics & Astronomy, The University of Alabama, Tuscaloosa, AL 35487, USA
[5] Department of Physics, University of Warwick, Coventry, CV4 7AL, UK
[6] Department of Physics and Astronomy, University of North Carolina, Chapel Hill, NC 27599-3255, USA
[7] Department of Physics, Middlebury College, Middlebury, VT 05753, USA
[8] Department of Astronomy, Columbia University, 550 West 120th Street, New York, NY 10027, USA
[9] CBA-Wilts, 2 Spa Close, Highworth, Swindon, Wilts SN6 7PJ, UK
Received 2014 May 15; accepted 2016 February 16; published 2016 April 4

ABSTRACT

Time-series photometry on the cataclysmic variable V455 Andromedae (hereafter V455 And, HS 2331+3905) reveals a rotation period shorter than the orbital period, implying the presence of a magnetic field. We expect that this magnetic field channels the accreted matter from the disk toward the white dwarf poles, classifying it as an Intermediate Polar. The two polar spinning emission areas are visible in the lightcurves at the rotation period of $67.61970396 \pm 0.00000072$ s, and its harmonic. Using photometric observations of V455 And obtained from 2007 October to 2015, we derive 3σ upper limits to the rate of change of the spin harmonic (SH) with time to be $dP_{\rm SH}/dt \leqslant -7.5 \times 10^{-15}$ s s^{-1} employing the *O–C* method, and -5.4×10^{-15} s s^{-1} with a direct nonlinear least squares fit. There is no significant detection of a changing spin period for the duration of 2007 October–2015. The 3σ upper limit for the rate of change of spin period with time is $dP_{\rm spin}/dt \leqslant -10.8 \times 10^{-15}$ s s^{-1} or -0.34 μs yr^{-1}. V455 And underwent a large-amplitude dwarf nova outburst in 2007 September. The pre-outburst data reflect a period 4.8 ± 2.2 μs longer than the best-fit post-outburst spin period. The angular momentum gained by the white dwarf from matter accreted during outburst and its slight subsequent shrinking should both cause the star to spin slightly faster after the outburst. We estimate that the change in spin period due to the outburst should be 5 μs, consistent with the empirical determination of 4.8 ± 2.2 μs (3σ upper limit of 11.4 μs).

Key words: novae, cataclysmic variables – stars: dwarf novae – stars: individual (V455 And, HS 2331+3905) – stars: variables: general – white dwarfs

1. INTRODUCTION

A large percentage of stars exist in binary configurations, and many interesting objects such as novae, millisecond pulsars, supersoft X-ray binaries, galactic black hole binaries and SNe Ia form due to binary interactions, mainly in the form of mass transfer. While these objects are well studied, the concept of binary evolution, which is fundamental to stellar astrophysics, remains poorly explored. Loss of angular momentum is one of the primary drivers of evolution for interacting stars, which commonly evolve into white dwarfs. A significant number of close binary interactions result in the formation of cataclysmic variables, which start out as two main sequence stars evolving through a common envelope phase (when the more massive star becomes a giant) that decreases their separation, reducing the orbital period to hours via a loss of angular momentum (Warner 1995). Eventually, the late-type main sequence donor (secondary) star fills its shrinking Roche lobe and transfers mass via the inner Lagrangian point to the accreting star, which has become a white dwarf (primary).

The dominant loss of angular momentum is initially via magnetic braking, which involves field lines capturing ionized matter lost in stellar wind and forcing it to revolve at the same angular velocity as the tidally locked donor star, thus extracting angular momentum from the orbit. Magnetic braking is thought to cease when the donor becomes fully convective (Taam & Spruit 1989), because the interface between the radiative core and the convective envelope plays a key role in the generation of the magnetic field (McDermott & Taam 1989). Disruption of the magnetic braking explains the observed period gap for cataclysmic variables (Davis et al. 2008). Subsequently, the loss of angular momentum is dominated by the emission of gravitational radiation when the orbital period becomes less than two hours. Cataclysmic variables containing white dwarfs with hydrogen dominated atmospheres evolve to an orbital period minimum near 70 minutes (e.g., Gänsicke et al. 2009), while those with helium dominated atmospheres achieve even shorter periods of less than an hour (e.g., Nelemans 2005; Breedt et al. 2012). Subsequently, the secondary becomes degenerate and its Kelvin–Helmoltz timescale becomes longer than the mass transfer timescale, driving it out of thermal equilibrium; both these effects cause the orbital period to increase. The short orbital periods, nearby distances of cataclysmic variables, and the visibility of the component stars make them a prime laboratory to study the effects of angular momentum losses on stellar evolution.

Binary population models (e.g., Kolb & Baraffe 1999; Howell et al. 2001b) are popular tools to investigate the global outcomes of close binary evolution, but are difficult to test through observations because of theoretical uncertainties in the physics of the common envelope and angular momentum losses, as well as observational selection effects. The Sloan Digital Sky Survey provided the first homogeneous sample of

[10] Hubble Fellow.

cataclysmic variables faint enough to detect the systems with short orbital periods (Anderson et al. 2008; Szkody et al. 2011). Followup observations that determined the orbital periods confirmed the general scenario of angular momentum losses, also revealing the orbital period minimum and a small number of systems with periods below 2 hr (Gänsicke et al. 2009). Work by Knigge et al. (2011) on donor radii in cataclysmic variables suggests additional angular momentum losses at short orbital periods than predicted by gravitational radiation alone. Thus, the physical parameters of the cataclysmic variables near the orbital period minimum and their angular momentum losses are critical to unraveling binary evolution and form the core goals of our study. Before we can begin to understand supernovae Ia and their complexities (from not knowing their progenitors, physics of the actual explosion, etc.), we must first understand the effects of accretion and angular momentum on the structure of a white dwarf.

1.1. Angular Momentum Evolution Near the Orbital Period Minimum

Durisen (1977) and recently Langer et al. (2000, 2002) theoretically demonstrated how accreting matter from the disk spins up the white dwarf in a cataclysmic variable. Ultra-violet *Hubble Space Telescope* (*HST*) observations confirm that accreting white dwarfs are observed to rotate faster than their non-interacting counterparts (Sion 1999), yet well below their break-up velocities. Angular momentum loss in nova explosions may prevent nonmagnetic CVs from reaching breakup (King et al. 1991). Tracking changes in the spin period addresses the question of how efficiently angular momentum is transferred to the core of the accreting white dwarf.

White dwarf rotation rates are important constraints for some models of SNe Ia (e.g., Piersanti et al. 2003; Yoon & Langer 2005). Calculations of the evolution of accreting white dwarfs through the ignition of hydrogen shell flashes shows material mixing, and indicates the importance of accreted angular momentum in rotation-induced mixing, relevant for the merger models of SNe Ia (Fujimoto & Iben 1997, pp. 245–252). Rapidly rotating progenitors may also lead to aspherical explosions, which could cause the observed polarization of SNe Ia (Howell et al. 2001a; Wang et al. 2003). Yoon & Langer (2005) demonstrate that white dwarf rotation rates play a role in the formation of millisecond pulsars and gamma-ray bursts that form from collapsing white dwarfs.

We are striving to gauge the rate of gain of angular momentum for an accreting white dwarf at the orbital period minumum. This period is where the mass transfer rates are the lowest $\sim 10^{-11}\,M_{\odot}\,\mathrm{yr}^{-1}$ for cataclysmic variables with accretion disks (Howell et al. 1995; Kolb & Baraffe 1999). Such a determination will contribute toward understanding the overall angular momentum evolution in an interacting binary, crucial from the perspective of binary evolution and stability.

1.2. A Unique Cataclysmic Variable: V455 And (HS 2331+3905)

Araujo-Betancor et al. (2005) conducted extensive photometric and spectroscopic observations of V455 And, which revealed that it is a cataclysmic variable with an orbital period of 81.1 minutes, unambiguously determined from the eclipses in its light curves. Bloemen et al. (2013) provide a recent spectroscopic measure of the spin period visible in the lightcurves at 67.619 s along with a prominent harmonic at 33.810 s, implying the presence of a magnetic field. This field disrupts the accretion disk near the white dwarf, and channels the accreted matter toward the poles, which get heated as a result of the accretion. This classifies V455 And as an intermediate polar.

Another periodicity is visible at 67.2 s with a harmonic at 33.6 s, closely spaced with the spin period at 67.619 s and its harmonic at 33.810 s. The beat period between these closely spaced components of 67.619 s and 67.2 s nearly corresponds with the observed spectroscopic period of 3.5 hr found from the radial velocity variations of the Balmer emission line wings (Araujo-Betancor et al. 2005). The source of this spectroscopic period is not understood, but it may be caused by a retrograde precession of a warp of the inner disc (see Armstrong et al. 2013).

The 2003 discovery data (Araujo-Betancor et al. 2005) also revealed short-timescale variability at 336.7 s, interpreted as nonradial white dwarf pulsations.[11] This accreting white dwarf pulsator V455 And in a binary near the orbital period minimum is unique as it has two independent clock mechanisms associated with the white dwarf: the spin period and the pulsation period. The longest stretch of time available for monitoring the system using the pulsation period as a clock is the interval between two outbursts[12], because an outburst effectively resets the clock. During an outburst, the white dwarf is heated to temperatures beyond the instability strip and can resume pulsations after a few years of cooling down to the blue edge of the instability strip. On the other hand, the spin period constitutes an ideal clock for long-term monitoring of the system.

Mauche (2004) measured the spin-up rate of the intermediate polar GK Per (1.9 day orbital period) as $0.27 \pm 0.05\ \mathrm{ms\ yr}^{-1}$ or $dP/dt = (-8.6 \pm 1.6) \times 10^{-12}\ \mathrm{s\ s}^{-1}$ for the spin period of 351.332 ± 0.002 s. Time-series photometry of the intermediate polar 1RXS J 070407+262501 (V418 Gem) revealed a spin period of 480.6700 s decreasing at the rate of $0.096 \pm 0.009\ \mathrm{ms\ yr}^{-1}$ or $(-3.04 \pm 0.29) \times 10^{-12}\ \mathrm{s\ s}^{-1}$ (Patterson et al. 2011). There are other measurements in the literature for cataclysmic variables such as EX Hya, FO Aqr, PQ Gem, AE Aqr, BG CMi, and DQ Her (Lamb & Patterson 1983; Shafter & Macry 1987; de Jager et al. 1994; Andronov et al. 2005; Kim et al. 2005; Evans et al. 2006; Andronov & Breus 2013). However, our project with V455 And constitutes the first such determination near the orbital period minimum with low mass transfer rates of $\sim 10^{-11}\,M_{\odot}\,\mathrm{yr}^{-1}$.

In the next few sections, we will describe our annual observations of V455 And and data reduction. This will be followed by the determination of the rate of change of spin

[11] Szkody et al. (2013) have shown that V455 And revealed variability near 250 s in 2009, two years after outburst. As the star cooled to quiescence, the variability was observed at longer and longer periods until the 2012 October data reflected power near 320–330 s. Although the evident long-term stability of the observed variability and the observation of longer periods with stellar cooling are suggestive of pulsations in the system, *HST* time-series spectroscopy revealed that the periodicity was present only in the lines and not in the continuum, casting doubt on their identification as non-radial pulsations.

[12] The long-term stability of a given pulsation period is related to its driving and damping, but short-period pulsators with 100–300 s periods near the blue edge of the instability strip are typically found to be stable on the timescales of at least decades (Clemens 1993; Kepler et al. 2005; Mukadam et al. 2006, 2013).

Table 1
Journal of Recent Photometric Observations Acquired at Apache Point Observatory

Telescope Aperture	Instrument	Start Time (TAI)	End Time (TAI)	Exposure Time (s)	Number of Images	Filter
3.5 m	Agile	2013 Sep 30 07:25:35	08:38:00	5	869	BG40
3.5 m	Agile	2013 Sep 30 08:38:35	10:26:45	5	1298	BG40
3.5 m	Agile	2013 Oct 1 01:48:09	01:51:59	5	46	BG40
3.5 m	Agile	2013 Oct 1 01:55:56	03:29:31	5	1123	BG40
3.5 m	Agile	2013 Oct 1 03:30:02	09:41:22	5	4456	BG40
3.5 m	Agile	2013 Oct 1 09:41:56	12:17:01	5	1861	BG40
3.5 m	Agile	2013 Oct 7 05:27:57	06:37:17	4	1040	BG40
3.5 m	Agile	2013 Oct 7 06:39:26	12:17:30	4	5071	BG40
3.5 m	Agile	2013 Oct 8 01:24:31	05:21:35	4	3556	BG40
3.5 m	Agile	2013 Oct 8 05:22:05	07:17:41	4	1734	BG40
3.5 m	Agile	2013 Oct 8 07:18:13	10:46:49	4	3129	BG40
3.5 m	Agile	2014 Nov 23 00:58:29	01:08:09	4	146	BG40
3.5 m	Agile	2014 Nov 23 1:46:12	03:10:48	4	1270	BG40
3.5 m	Agile	2014 Nov 23 03:16:49	06:46:29	4	3146	BG40
3.5 m	Agile	2014 Nov 23 06:47:05	09:42:25	4	2631	BG40
3.5 m	Agile	2015 Sep 12 08:24:00	12:10:10	5	2715	BG40
3.5 m	Agile	2015 Sep 13 07:24:51	12:13:19	4	4328	BG40
3.5 m	Agile	2015 Oct 10 05:05:57	07:50:01	4	2462	BG40
3.5 m	Agile	2015 Oct 11 01:24:21	05:35:01	4	3761	BG40
3.5 m	Agile	2015 Oct 11 05:45:26	06:07:42	4	335	BG40
3.5 m	Agile	2015 Oct 11 08:12:41	08:16:45	4	62	BG40
3.5 m	Agile	2015 Oct 11 08:20:03	12:18:31	4	3578	BG40

period with time using two established methods. Lastly, we will show the effect of the outburst on the spin period.

2. OBSERVATIONS

To deduce the spin-up rate of V455 And, we have been observing it annually at the 3.5 m telescope at Apache Point Observatory (APO) and the 2.1 m telescope at McDonald Observatory since 2007. We now have sufficient data on V455 And to derive meaningful constraints on its rate of change of spin period with time $dP_{\rm spin}/dt$, and intend to continue our long-term program with annual data acquisition.

We also have access to archival data on V455 And from 2003 to 2006. Most of the time-series photometry we include here has already been published elsewhere. The 2003 discovery data were published in Araujo-Betancor et al. (2005), the 2004–2006 data will be published shortly (S. Pyrzas et al. 2016, in preparation), while the 2007–2012 data have been published by Szkody et al. (2013). We include the journal of observations for our recently acquired time-series photometry in Table 1. These data were acquired at the 3.5 m APO telescope using the time-series photometer Agile (Mukadam et al. 2011).

We used a standard IRAF[13] (Tody 1993) reduction to extract sky-subtracted light curves from the CCD frames using weighted circular aperture photometry (O'Donoghue et al. 2000). Next, we converted the data to fractional intensity ($\Delta I/I$) and the mid-exposure times of the CCD images to Barycentric Dynamic Time (TDB). We show the reduced lightcurves from 2015 in the left panels of Figure 1.

[13] IRAF is distributed by the National Optical Astronomy Observatories, which are operated by the Association of Universities for Research in Astronomy, Inc., under cooperative agreement with the National Science Foundation.

Dividing the new and archival reduced data into closely-spaced groups or seasons, we computed Discrete Fourier Transforms (DFTs) of all possible seasons to check whether the 33.8 s period was cleanly resolved from the 33.6 s alias in order to obtain reliable phases. We are choosing to focus on the 33.8 s power structure since it has twice the separation of the 67.6 s power, making it easier to resolve. Figure 1 shows the DFTs for the 2015 September and October seasons in the right-hand panels, and the corresponding best-fit periodicities in Table 2. The nonlinear least squares analysis and the determination of the 1σ Monte-Carlo uncertainties shown were conducted using the program Period04 (Lenz & Breger 2005). Only the seasons with cleanly resolved periods have been included in the O–C analysis presented in the subsequent section.

3. DETERMINING THE RATE OF CHANGE OF SPIN PERIOD WITH TIME

Our goal is to isolate the evolutionary rate of change of spin period with time due to the gain in angular momentum. In order to do so, we need to understand and explore other causes of orbital time delays that may affect our measurements. We will subsequently use the O–C technique to obtain the rate of change of spin period with time, and refine that determination with a direct nonlinear least squares fit.

3.1. Orbital Motion of the Spin Clock

Note that the rotating and revolving white dwarf constitutes a clock in orbit; the changing light travel time during an orbit is reflected in the pulse arrival times. The observed phase of the clock (O) compared to the phase of a stationary clock at the same period (C) should show a modulation at the orbital period

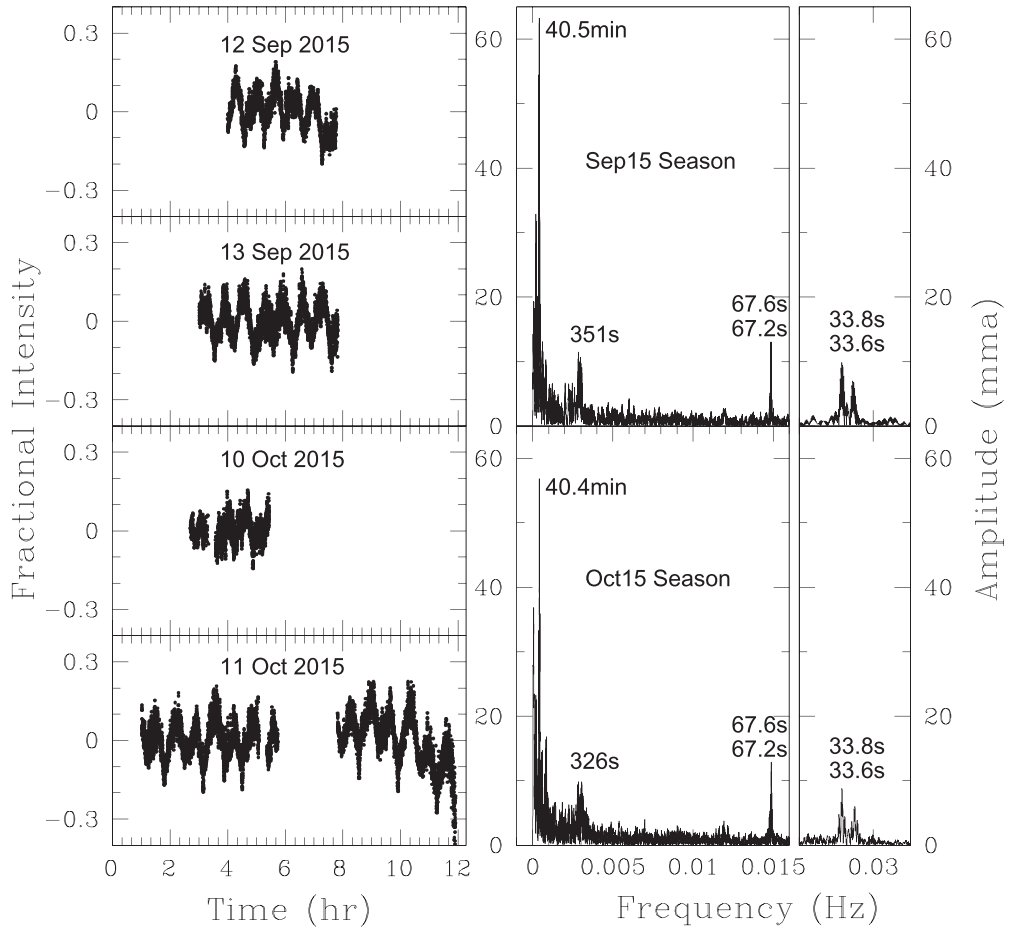

Figure 1. Recent Data on V455 And obtained in 2015 using the 3.5 m telescope at Apache Point Observatory.

(e.g., Winget et al. 2003; Mullally et al. 2008; Hermes et al. 2010; Hermes 2013). Mukadam et al. (2015) have derived the amplitude of the *O–C* modulation $\mathrm{OCM_{amp}}$ to be expected from a stellar clock in an elliptical orbit to be:

$$\mathrm{OCM_{amp}} = \frac{a\sin(i)}{c}(1 - e\cos(E)) \quad (1)$$

where a is the semimajor axis of the elliptical orbit, i is the angle of inclination, e is the ellipticity, and E is the eccentric anomaly. Using the grazing eclipses present in the lightcurve, Araujo-Betancor et al. (2005) deduce the inclination angle of the system i to be 75°. Folding the detrended radial velocities over the orbital period of 81.08 minutes, Araujo-Betancor et al. (2005) find a sinusoidal radial velocity curve, implying no significant deviation from a circular orbit. Theoretically, a circular orbit can be expected in such a short-period tidally locked binary. Assuming a white dwarf mass of $0.6\,M_{\odot}$ and a secondary mass of $0.07\,M_{\odot}$ (Araujo-Betancor et al. 2005), we can then deduce the value of the semimajor axis a using Kepler's equations. The radius of the white dwarf's orbit can then be computed as $a_{\mathrm{wd}} = (0.07/0.67)a = 3.94 \times 10^7$ m. The amplitude of the *O–C* modulation due to the orbital motion of the white dwarf then becomes 0.13 s, easily swamped by the uncertainties in phase.

In a simple estimation, compensating for the orbital variation in light travel times could remove 0.13 s of uncertainty, reducing the lowest uncertainty presented in Table 3 of 0.29 s to approximately 0.26 s, not a significant improvement. This implies that the orbital motion of the white dwarf around the center of mass of the system can be presently ignored in constraining the evolution of the spin period with existing data.

3.2. *O–C* Diagram

The *O–C* technique can be used to improve the period estimate for any periodic phenomenon, where *O* stands for the observed phase. The observed phase is typically determined by subjecting the lightcurve to a linear least squares fit using a sinusoid of fixed period *P*, with *O* being the time of the first zero crossing in our case. The corresponding ephemeris calculated assuming that the period *P* is constant is denoted by *C*. Any linear trend in the *O–C* diagram can be used to rectify the period estimate with a correction ΔP, while a nonlinear trend is suggestive of a variable period. The larger the change in the period, the larger the discrepancy *O–C*. The longer the timebase of the observations, the larger the discrepancy *O–C* due to the drifting period. The *O–C* technique is much more sensitive than the direct method of plotting period as a function of time; this is because it has the advantage of adding up the discrepancy *O–C* over the entire timebase of observations consisting of numerous cycles. Neglecting higher order terms, Kepler et al. (1991) showed the derivation of the following *O–C* equation using a Taylor series expansion of the

Table 2
Best-fit Periodicities with Their 1σ Monte Carlo Uncertainties for the 2013–2015 Seasons

Season	Period	Amplitude (mma)[a]
2013 Sep	4.615 ± 0.021 hr	19.19 ± 0.88
	79.797 ± 0.051 minutes	26.1 ± 1.0
	40.51 ± 0.44 minutes	49.4 ± 4.2
	26.9562 ± 0.0052 minutes	18.41 ± 0.42
	20.3 ± 1.6 minutes	15.4 ± 5.4
	311.081 ± 0.022 s	10.87 ± 0.63
	67.620 ± 0.063 s	4.5 ± 1.1
	67.2677 ± 0.0011 s	16.40 ± 0.18
	33.80985 ± 0.00041 s	8.88 ± 0.73
	33.63397 ± 0.00044 s	6.64 ± 0.99
2013 Oct	3.7753 ± 0.0054 hr	25.03 ± 0.24
	80.395 ± 0.038 minutes	26.74 ± 0.50
	40.4317 ± 0.0026 minutes	55.54 ± 0.66
	26.8477 ± 0.0056 minutes	13.26 ± 0.61
	20.2068 ± 0.0030 minutes	14.93 ± 0.54
	321.966 ± 0.019 s	9.02 ± 0.53
	67.620 ± 0.059 s	5.7 ± 1.8
	67.26504 ± 0.00065 s	16.71 ± 0.58
	33.8100 ± 0.0048 s	9.8 ± 1.3
	33.63241 ± 0.00033 s	8.00 ± 0.73
2014 Nov	81.16 ± 0.15 minutes	48.0 ± 1.0
	40.560 ± 0.032 minutes	60.5 ± 1.0
	20.140 ± 0.020 minutes	20.33 ± 0.97
	345.4 ± 4.3 s	11.3 ± 1.7
	67.6 ± 1.4 s	6.9 ± 6.8
	67.294 ± 0.021	13.6 ± 7.1
	33.81 ± 0.66	10 ± 12
	33.65 ± 0.21	7 ± 11
2015 Sep	80.690 ± 0.043	27.15 ± 0.86
	40.4558 ± 0.0042	61.82 ± 0.83
	351.178 ± 0.029	11.49 ± 0.79
	67.62 ± 0.43	5.9 ± 2.0
	67.2582 ± 0.0010	13.7 ± 1.0
	33.80947 ± 0.00042	9.75 ± 0.92
	33.62901 ± 0.00053	6.69 ± 0.81
2015 Oct	5.5 ± 1.1 hr	46.6 ± 6.7
	67.033 ± 0.042	26.5 ± 1.2
	40.4337 ± 0.0080	60.82 ± 0.97
	27.0 ± 2.3	12.3 ± 4.2
	20.25 ± 0.83	16.9 ± 2.0
	326.3 ± 5.3	9.7 ± 3.5
	67.6176 ± 0.0028	6.05 ± 0.86
	67.2457 ± 0.0013	13.26 ± 0.82
	33.80992 ± 0.00046	8.82 ± 0.78
	33.610 ± 0.049	5.9 ± 1.6

Note.
[a] One milli modulation amplitude (mma) equals 0.1% change in intensity.

phase of a slowly changing period:

$$O\text{–}C = \Delta E_0 + \Delta P\, E + \frac{1}{2}\, P\, \frac{dP}{dt}\, E^2 \qquad (2)$$

where E_0 is the reference zero epoch and E gives the epoch or cycle count.

There are two essential requirements in successfully constructing an O–C diagram for a given period. In order to obtain reliable observed phases, the period must be well resolved in multiple seasons or data sets. Second, the cycle counts between these sets of observations must be unambiguously determined to obtain reliable calculated phases. Figure 2 shows that the 33.8 s harmonic is resolved from the nearby alias at 33.6 s. We are thus able to fulfill both requirements for the 33.8 s harmonic, and construct the corresponding O–C diagram. We are unable to phase the 33.6 s period over our database due to its intrinsic low coherence (Gänsicke 2007). This is also noticeable in Figure 2, where the peaks are sometimes at periods lower than 33.6 s and sometimes at periods higher than 33.6 s.

Table 3
O–C Values for the 33.80985198 s Period with Their 1σ Monte Carlo Uncertainties[a]

Season	O (TDB)	σ_O (s)	Epoch	O–C (s)
2003	2452866.459424	0.74	−3927965	-2.2 ± 1.4[b]
2004	2453241.332852	0.32	−2969988	1.34 ± 0.62
2006	2453968.292450	0.68	−1112266	4.7 ± 1.7[b]
2007 Oct	2454403.541803	0.29	0	0.00 ± 0.29
2010 Sep	2455446.593734	0.43	2665486	-0.22 ± 0.64
2010 Oct	2455481.840128	0.48	2755557	1.03 ± 0.69
2011	2455829.580704	0.45	3644197	-0.11 ± 0.80
2012	2456213.574141	0.45	4625480	-0.06 ± 0.95
2013 Sep	2456565.814484	0.45	5525619	-0.8 ± 1.1
2013 Oct	2456572.732989	0.35	5543299	-0.1 ± 1.1
2014 Nov	2456984.544435	0.52	6595670	1.0 ± 1.3
2015 Sep	2457277.854656	0.46	7345215	-1.33 ± 1.4
2015 Oct	2457305.717662	0.51	7416418	-0.55 ± 1.4

Notes.
[a] In seasons where the resolution of the 33.6 s and 33.8 s components is not entirely complete, the uncertainties can be under-estimated because the beat phase dominates over the phase of the individual mode in a short lightcurve.
[b] Uncertainties due to manual synchronization of the Kryoneri data acquisition computer to a GPS clock were added in quadrature to the Monte Carlo uncertainties to obtain these realistic error bars for the 2003 and 2006 seasons of observation.

The frequency splitting between the 67.6 s and 67.2 s periods is half as much as that of the 33.8 s and 33.6 s periods, as shown by a comparison of the left and right panels in Figure 2. Figure 2 also shows seasons where the spin period is not clearly resolved, and which cannot be included in the construction of its O–C diagram. Also, our observations contain half as many cycles for the spin period compared to the harmonic, implying relatively larger uncertainties in the observed phases for seasons where the spin period is resolved from the nearby 67.2 s alias. Both these reasons explain how any O–C diagram for the spin period would contain fewer points compared to the O–C diagram for the 33.8 s harmonic and relatively greater uncertainties for those few points, thereby introducing an ambiguity in the cycle counts between usable seasons and making it impossible to construct a reliable O–C diagram for the spin period. Note that it is possible to use the cycle counts between seasons for the 33.8 s harmonic to determine the cycle counts for the 67.6 s period, but that does not lead to an independent constraint, only a less reliable dependent constraint. We will henceforth focus our efforts on measuring dP/dt for just the 33.8 s harmonic of the spin period.

Note that in order to account for the other frequencies, we simultaneously fit all significant periods of variability to each of the seasons of observations using Period04 (Lenz &

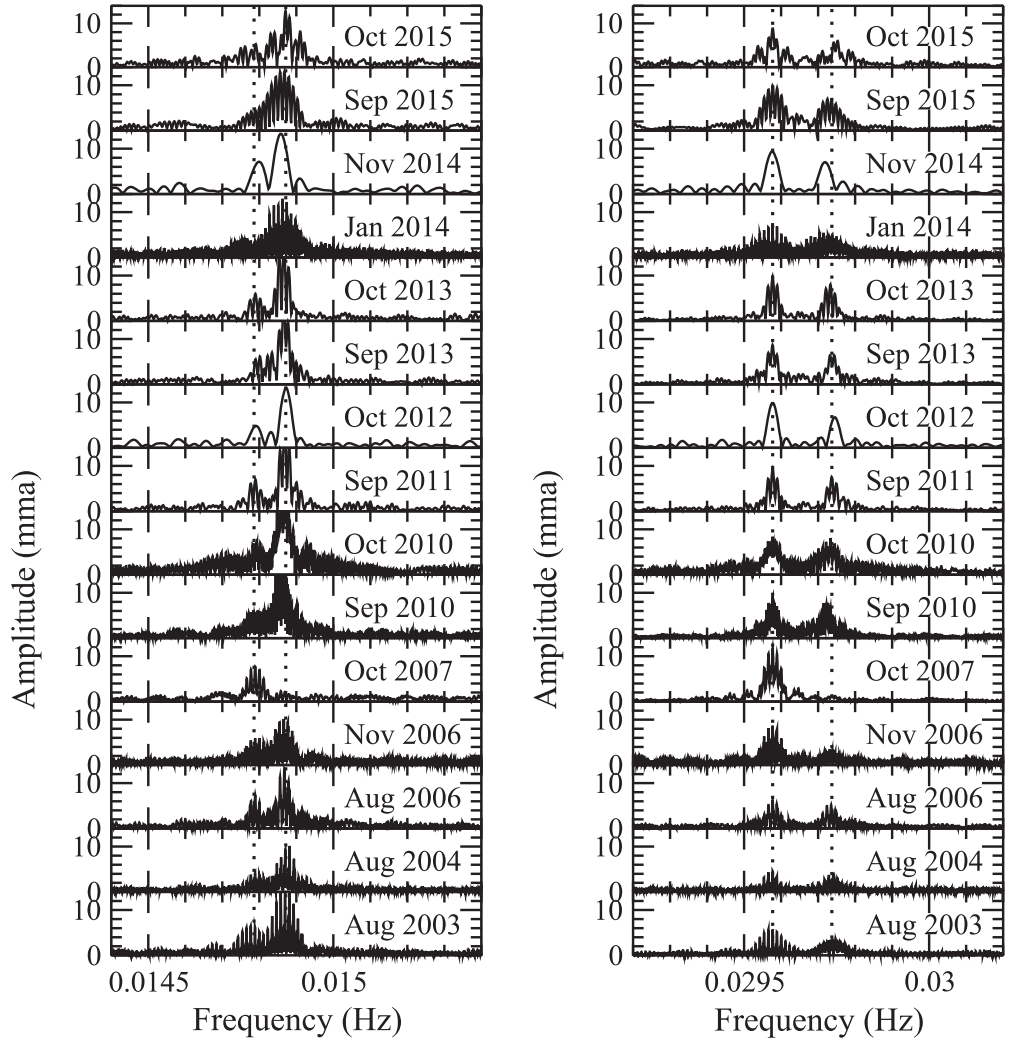

Figure 2. The left-hand panels indicate that the 67.6 s period is not always clearly resolved from the nearby alias at 67.2 s, implying that all the seasons of observations shown cannot be used to obtain reliable phases for the construction of its *O–C* diagram. The right-hand panels show that the 33.8 s harmonic of the spin period is clearly resolved from the nearby alias at 33.6 s in all the seasons of observations used to construct its *O–C* diagram.

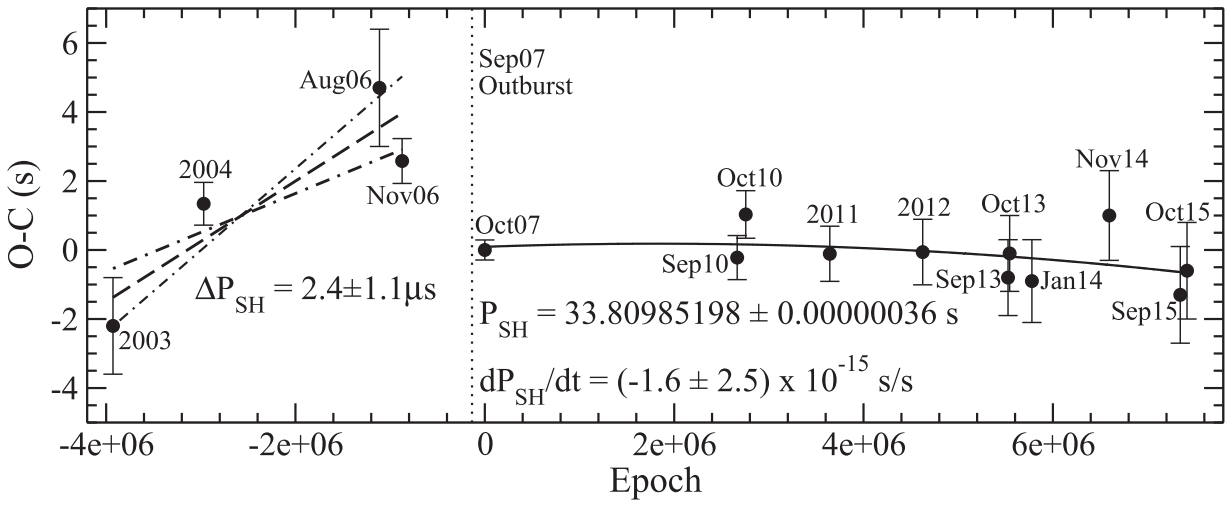

Figure 3. We show the *O–C* diagram for the 33.80985198 s harmonic with the solid line indicating the post-outburst best-fit parabola, while the dashed line reveals the best-fit correction of 2.4 μs to the pre-outburst harmonic period, and the dashed–dotted lines indicate the minimum and maximum slopes possible, yielding realistic uncertainties. This implies that the pre-outburst spin period was longer than the post-outburst fit by 4.8 ± 2.2 μs (3σ upper limit of 11.4 μs).

Breger 2005). We show the discrepancy O–C obtained as a function of the cycle count or epoch E in Figure 3, as well as list these values in Table 3. The Table 3 also indicates the absolute observed phase (first time of zero crossing or first minimum) and its 1σ Monte Carlo uncertainty, so our results can be reproduced and/or improved with the addition of other observations.

A parabolic least squares fit to the post-outburst points in the O–C diagram yields the following value for the rate of change of period with time: $dP_{\rm SH}/dt = (-1.6 \pm 2.5) \times 10^{-15}$ s s^{-1} for the period $33.80985198 \pm 0.00000036$ s.

Note that the above best-fit to the O–C diagram is unweighted. The uncertainty in period also governs the true uncertainty of a point in the O–C diagram, with both an explicit (uncertainty in C) and an implicit (uncertainty in O) dependence. When there are closely spaced components such as the 33.8 s and 33.6 s periods, their clean resolution is key in determining reliable phases. In seasons where the resolution is not entirely complete, the true uncertainty is not reflected in the Monte Carlo error bar in the O–C diagram, because the beat phase dominates over the phase of the individual mode in a short lightcurve. Since we cannot completely trust the errors listed in Table 3, we do not favor a weighted fit.

During the first stage of using the O–C method, the value of the period P improves linearly with the cycle count E as the first order term is dominant. Eventually, the second-order term becomes important provided there is a non-zero detectable change in the period. The constraints on the value of $dP_{\rm SH}/dt$ then become meaningful and improve with the square of the timebase. We are still in the first stage, where the value of period is determined to a high accuracy, and the value of $dP_{\rm SH}/dt$ from the parabolic fit is rudimentary with the error bar being more significant than the value itself. Hence, we derive a 3σ upper limit to the rate of change of period with time as $dP_{\rm SH}/dt \leqslant -7.5 \times 10^{-15}$ s s^{-1} using the O–C diagram.

3.3. Direct Nonlinear Least Squares Method

The direct nonlinear least squares method involves optimizing the drift rate dP/dt obtained using the O–C diagram; it is not independent of the O–C method. This technique is about fitting a single variable period with a dP/dt term to all the data from 2007 to 2015 October with a fixed amplitude, while varying the period, dP/dt value, and phase to minimize the residuals. Since we are fitting several years of data simultaneously, each periodicity including closely spaced values are very well resolved, eliminating the need to fit all periodicities simultaneously.

This approach converges only to the local minimum (near the value obtained by the O–C method) and does not determine the global minimum. This program named Nonlinear Least SQuares Period Derivative (NLSQPD) has the following advantages over the O–C technique: it simultaneously fits every cycle, while also being able to utilize isolated observations that do not resolve the 33.8 s and 33.6 s periods. For the nine year baseline from 2007 October to 2015, all the available data listed in Table 3 constitute well-resolved seasons. In other words, both the O–C diagram and the NLSQPD program are being subject to exactly the same data set.

Using the NLSQPD program on a nine year lightcurve of V455 And from 2007 October to 2015, we determine a drift rate of $(-0.7 \pm 1.8) \times 10^{-15}$ s s^{-1} for the 33.80985198 s period. Since every cycle is fit simultaneously, it is a better technique than the O–C method. Hence we adopt this determination as our best value, and conclude that the drift rate for the $67.61970396 \pm 0.00000072$ s spin period can be constrained as $(-1.4 \pm 3.6) \times 10^{-15}$ s s^{-1}. Note that within the uncertainties, the drift rate could also be zero, implying that we do not detect a significant variation in the spin period for the duration of 2007 October–2015. Hence, we adopt a 3σ upper limit for the rate of change of spin period as -10.8×10^{-15} s s^{-1}.

4. OUTBURST OF 2007 SEPTEMBER

On the fourth of 2007 September, V455 And underwent a superoutburst (Senziani et al. 2008; Maehara et al. 2009; Nogami et al. 2009). During the outburst, the brightness was found to increase by 8 mag from the quiescent magnitude of $V = 16.5$ to the maximum of $V = 8.5$. There was no evidence of superhumps or humps during the rapid rising phase. At the maximum brightness, early superhumps were observed with a period of 81 minutes, i.e., the orbital period. Several days after the maximum brightness, superhumps with a period of 82.4 minutes were observed. According to Maehara et al. (2009), the system revealed a fading trend of 0.03 mag day^{-1} after the initial rapid decline in brightness. The spin period disappeared from the light curves for a month after the outburst as the accretion disk dominated the light from the system, but it was seen in observations acquired in 2007 October (Szkody et al. 2013).

Using the pre-outburst seasons of observation on V455 And, we are able to establish a thirteen year database from the discovery data of 2003 until the recent 2015 data that include the 2007 September outburst. The pre-outburst data were primarily acquired in white light, while the post-outburst observations were acquired using the wide band BG40 filter. Hellier et al. (1994) demonstrate that pulse profiles for the intermediate polar RE 0751+14 are quasi-sinusoidal in the blue, but double-peaked in the red. Figure 4 shows the folded pulse shapes for all our seasonal data, and clearly demonstrates that apart from small amplitude changes, there are no other major changes in the pulse profiles from season to season.

Figure 3 shows the O–C values based on all of our seasons from 2003 to 2015. Note that the pre- and post-outburst data actually constitute two independent O–C diagrams. It is possible to fit a straight line to the 2003–2006 points with a slope of $(2.37 \pm 0.27) \times 10^{-6}$ s, thus correcting the pre-outburst period to 33.80985435 s. To reiterate, we fit the post-outburst phases alone with a parabola to determine a value for the spin period. We also used the pre-outburst phases alone to determine a value for the spin period before outburst. We are comparing the post-outburst spin period with the pre-outburst spin period to insinuate a change in the spin period due to the outburst. At this juncture, we are not comparing the pre- and post-outburst phases directly, and hence any possible minor color dependence of the phases is irrelevant. We emphasize this point as the pre-outburst data were acquired in white light and the post-outburst observations were acquired with a BG40 filter.

The change in the period of the spin harmonic due to the outburst must be taken with a grain of salt due to the larger uncertainty of the 2003 and 2006 O–C points, which dictate the above determination. These data were mainly acquired at Kryoneri observatory, where the clock of the data acquisition

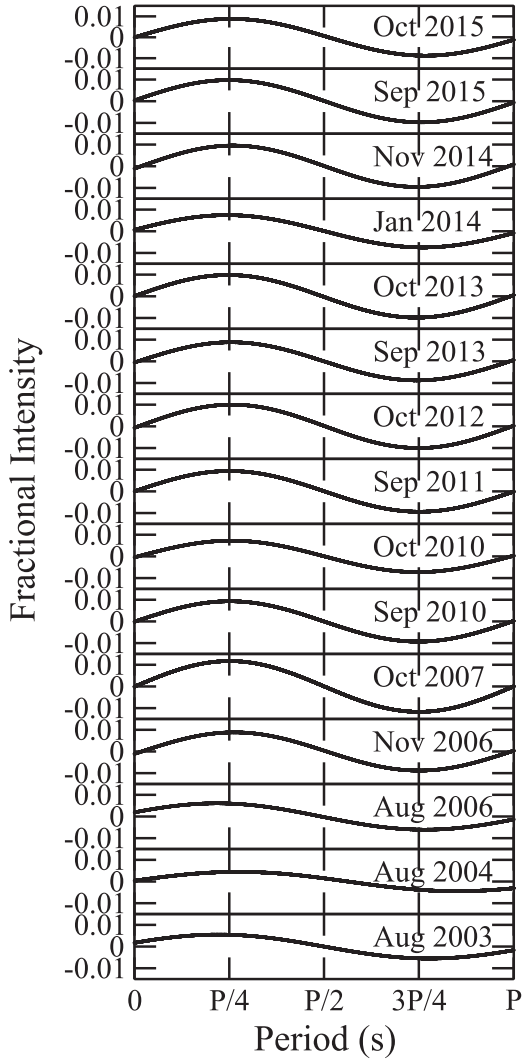

Figure 4. We show the pulse profiles of all our seasonal data from 2003 to 2015, folded on the period 33.80985198 s using the observed phases listed in Table 3. Apart from small changes in amplitude, no other significant changes are visible even when comparing the 2003–2006 seasons acquired in white light with the 2007–2015 data acquired using the wide band BG40 filter.

computer must be set manually to synchronize it with the GPS clock. Most trained observers can do so with a precision of better than a second. For the purpose of determining realistic uncertainties, we will adopt a limited accuracy of 2–3 s for the process of synchronization. Note that should we assume the Kryoneri observer made a mistake in syncing the two clocks by 3–4 s each night, the combined seasonal lightcurve does not converge. As we had no convergence problems with the real data, we assume that the observer synchronized the data acquisition computer with the GPS clock to better than 2–3 s.

We ran simulations shifting individual nights in the 2003 and 2006 seasons by 2–3 s, and determined the net change in the *O–C* phases to be about 0.7 s for the 2003 data and 1.2 s for the 2006 data. To be conservative, we additionally boost these determinations to 1.0 s for the 2003 season and 1.5 s for the 2006 season. Adding these uncertainties from clock synchronization in quadrature with the Monte Carlo uncertainties, yields relatively realistic error bars for these pre-outburst *O–C* points. Note that should the observer make an error of 3 s in the same direction every night, then the net phase shift expected in the *O–C* diagram would be 3 s. We have assumed in our simulations that sometimes the observer sets the clock ahead of time and sometimes after the time, creating a relative displacement of individual runs that contributes to the overall relative uncertainty in the combined run. We cannot estimate the abolute uncertainty in timing after the fact. However, the process of manual synchronization to the GPS clock every night serves as an absolute timing check.

Using the above determinations of realistic uncertainties for the 2003 and 2006 seasons, we can determine the minimum and maximum slopes possible for the pre-outburst linear fit (see Figure 3). This gives us reliable uncertainties, changing the difference between the pre- and post-outburst periods to $(2.4 \pm 1.1)\ \mu$s. The change between the pre- and post-outburst values of the spin period is then twice as large at $(4.8 \pm 2.2)\ \mu$s. To be additionally conservative, we adopt a 3σ upper limit of 11.4 μs.

4.1. Theoretical Estimation

Araujo-Betancor et al. (2005) determined the effective temperature of the primary white dwarf in V455 And at quiescence, and found a low value of 10,500 K. Townsley & Gänsicke (2009) find that the quiescent effective temperature provides one of the best available methods for predicting the angular momentum loss and resultant mass-transfer rate that dictate the evolution of a cataclysmic variable. The low effective temperature of the white dwarf in V455 And implies a low mean accretion rate (Townsley & Bildsten 2003; Townsley & Gänsicke 2009).

Let us assume that the white dwarf mainly accretes matter during outbursts, when the newly arrived material with more specific angular momentum than the white dwarf causes it to spin up slightly. Under this scenario, the white dwarf spin is expected to remain constant between outbursts. We can compute the approximate change in the white dwarf spin by assuming that the mass accreted during the dwarf nova outburst dM becomes attached to the magnetic field of the white dwarf at a radius, $r_{\rm orb}$. We assume that the value of $r_{\rm orb}$ is nearly twice the radius of the white dwarf star R, which is also close to the corotation radius with the disk. The change in the spin period of the white dwarf can then be estimated using the following equation.

$$dL = I\ d\omega + \omega\ dI \tag{3}$$

where $dL = dM\ r_{\rm orb}^2 \omega_{\rm orb} = dM\sqrt{GMr_{\rm orb}}$ is the angular momentum added by the accreted mass, I is the moment of inertia of the white dwarf, ω is its spin rate, and $\omega_{\rm orb}$ is the Keplerian angular frequency at $r_{\rm orb}$. As $R \propto M^{-1/3}$ is an appropriate approximation for the white dwarf mass-radius relation near a stellar mass of $M_{\rm WD} = 0.6 M_{\odot}$, we find that approximately $I \propto MR^2 \propto M^{1/3}$. We have assumed that the white dwarf rotates as a solid body due to its strong global magnetic field.

$$dL \approx I\ d\omega + \frac{I\omega}{3}\frac{dM}{M}. \tag{4}$$

The two terms in the above equation relate to the gain in angular momentum from the accreted mass and the slight shrinking of the white dwarf due to the added mass. By using a $0.6 M_{\odot}$ model white dwarf from the "wd_cool_0.6" test suite problem in the MESA stellar evolution code (Paxton et al. 2011), we compute the moment of inertia of the white

dwarf star as $I = 1.6 \times 10^{50}\,\mathrm{g\,cm^2}$, with a radius of 8.9×10^8 cm. Szkody et al. (2013) determined the post-outburst cooling curve for V455 And, which implied that the mass accreted during outburst was $dM \sim 1.5 \times 10^{-9}\,M_\odot$. Using these values in the relations above gives $d\omega/\omega \approx 7.4 \times 10^{-8}$ or a change in spin period of 5 μs, consistent with the empirical determination of 4.8 ± 2.2 μs (3σ upper limit of 11.4 μs).

Note that this value scales approximately as $r_{\mathrm{orb}}^{1/2}$, and so has a significant dependence on this assumed capture radius. Should the white dwarf in V455 And be in spin equilibrium, then Norton et al. (2004, 2008) find that the attachment point of matter from the disk to the white dwarf magnetic field, r_{orb}, is at approximately the co-rotation radius. Also, spin equilibrium would imply that any angular momentum added to the white dwarf during the outburst would be slowly extracted by the interaction of the magnetic field with the disk during accretion quiescence. In other words, this angular momentum must be coupled back into the disk and then into the orbit in order to be lost via gravitational radiation. If this process occurs smoothly over the inter-outburst time of a few decades, this would imply an average spin down rate of $dP/dt = -5 \times 10^{-15}\,\mathrm{s\,s^{-1}}$ assuming a 30 years inter-outburst duration. This value is smaller than the uncertainty of our current post-outburst constraint. However, this is a very simplistic picture, and the transfer of angular momentum back to the disk may occur on significantly longer timescales. For example, mass and angular momentum loss during nova outbursts may reduce the white dwarf spin below the equilibrium value, such that it must be spun back up. It is also possible that the white dwarf has yet to reach spin equilibrium, which may constrain its magnetic field, though the evolutionary calculations of Norton et al. (2008) do not appear to cover the required low-field region of parameter space.

5. CONCLUSION

Using a nine-year baseline of observations from 2007 to 2015 on V455 And, we derive a 3σ upper limit to the rate of change of the $67.61970396 \pm 0.00000072$ s spin period with time to be $-10.8 \times 10^{-15}\,\mathrm{s\,s^{-1}}$ or -0.34 $\mu\mathrm{s\,yr^{-1}}$. Despite their relatively larger uncertainties, the pre-outburst data are suggestive of a spin period larger than the post-outburst value by (4.8 ± 2.2) μs. Accretion and angular momentum gain during outburst, followed by subsequent shrinking of the white dwarf, should cause a $0.6\,M_\odot$ star to spin faster by 5 μs. This theoretical expectation is consistent with the empirical determination of 4.8 ± 2.2 μs (3σ upper limit of 11.4 μs), thus providing rudimentary evidence of a change in spin period due to a dwarf nova outburst.

A.S.M. and P.S. acknowledge funding support for this project from NSF grants AST-1514737 and AST-1008734 as well as NASA HST-GO-12231.01-A through the Space Telescope Science Institute, which is operated by the Association of Universities for Research in Astronomy, Inc., under NASA contract NAS 5-26555. The research leading to these results has received funding from the European Research Council under the European Union's Seventh Framework Programme (FP/2007-2013)/ERC Grant Agreement No. 320964 (WDTracer). Support for this work was also provided by NASA through the Hubble Fellowship grant #HST-HF2-51357.001-A, awarded by the Space Telescope Science Institute, which is operated by the Association of Universities for Research in Astronomy, Incorporated, under NASA contract NAS5-26555.

REFERENCES

Anderson, S. F., Becker, A. C., Haggard, D., et al. 2008, AJ, 135, 2108
Andronov, I. L., & Breus, V. V. 2013, Ap, 56, 518
Andronov, I. L., Ostrova, N. I., & Burwitz, V. 2005, in ASP Conf. Ser. 335, The Light-Time Effect in Astrophysics: Causes and cures of the O-C diagram, ed. C. Sterken (San Francisco, CA: ASP), 229
Araujo-Betancor, S., Gänsicke, B. T., Hagen, H.-J., et al. 2005, A&A, 430, 629
Armstrong, E., Patterson, J., Michelsen, E., et al. 2013, MNRAS, 435, 707
Bloemen, S., Steeghs, D., De Smedt, K., et al. 2013, MNRAS, 429, 3433
Breedt, E., Gänsicke, B. T., Marsh, T. R., et al. 2012, MNRAS, 425, 2548
Clemens, J. C. 1993, BaltA, 2, 407
Davis, P. J., Kolb, U., Willems, B., & Gänsicke, B. T. 2008, MNRAS, 389, 1563
de Jager, O. C., Meintjes, P. J., O'Donoghue, D., & Robinson, E. L. 1994, MNRAS, 267, 577
Durisen, R. H. 1977, ApJ, 213, 145
Evans, P. A., Hellier, C., & Ramsay, G. 2006, MNRAS, 369, 1229
Fujimoto, M. Y., & Iben, I., Jr. 1997, Stellar Ecology: Advances in Stellar Evolution, ed. R. T. Rood, & A. Renzini (New York: Cambridge Univ. Press)
Gänsicke, B. T. 2007, in ASP Conf. Ser. 372, 15th European Workshop on White Dwarfs, ed. R. Napiwotzki, & M. R. Burleigh (San Francisco, CA: ASP), 597
Gänsicke, B. T., Dillon, M., Southworth, J., et al. 2009, MNRAS, 397, 2170
Hellier, C., Ramseyer, T. F., & Jablonski, F. J. 1994, MNRAS, 271, L25
Hermes, J. J. 2013, BAAS, 221, 424.04
Hermes, J. J., Mullally, F., Winget, D. E., et al. 2010, in AIP Con. Ser. 1273, 17th European White Dwarf Workshop, ed. K. Werner, & T. Rauch (Melville, NY: AIP), 446
Howell, D. A., Höflich, P., Wang, L., & Wheeler, J. C. 2001a, ApJ, 556, 302
Howell, S. B., Nelson, L. A., & Rappaport, S. 2001b, ApJ, 550, 897
Howell, S. B., Szkody, P., & Cannizzo, J. K. 1995, ApJ, 439, 337
Kepler, S. O., Costa, J. E. S., Castanheira, B. G., et al. 2005, ApJ, 634, 1311
Kepler, S. O., Winget, D. E., Nather, R. E., et al. 1991, ApJL, 378, L45
Kim, Y. G., Andronov, I. L., Park, S. S., & Jeon, Y.-B. 2005, A&A, 441, 663
King, A. R., Regev, O., & Wynn, G. A. 1991, MNRAS, 251, 30P
Knigge, C., Baraffe, I., & Patterson, J. 2011, ApJS, 194, 28
Kolb, U., & Baraffe, I. 1999, MNRAS, 309, 1034
Lamb, D. Q., & Patterson, J. 1983, in IAU Coll. 72: Cataclysmic Variables and Related Objects, Vol. 101, ed. M. Livio, & G. Shaviv (Dordrecht: Springer), 229
Langer, N., Deutschmann, A., Wellstein, S., & Höflich, P. 2000, A&A, 362, 1046
Langer, N., Yoon, S.-C., Wellstein, S., & Scheithauer, S. 2002, in ASP Conf. Ser. 261, The Physics of Cataclysmic Variables and Related Objects, ed. B. T. Gänsicke, K. Beuermann, & K. Reinsch (San Francisco, CA: ASP), 252
Lenz, P., & Breger, M. 2005, CoAst, 146, 53
Maehara, H., Imada, A., Kubota, K., et al. 2009, in ASP Conf. Ser. 404, The Eighth Pacific Rim Conf. on Stellar Astrophysics: A Tribute to Kam-Ching Leung, ed. B. Soonthornthum et al. (San Francisco, CA: ASP), 57
Mauche, C. W. 2004, in ASP Conf. Ser. 315, IAU Coll. 190: Magnetic Cataclysmic Variables, ed. S. Vrielmann, & M. Cropper (San Francisco, CA: ASP), 120
McDermott, P. N., & Taam, R. E. 1989, ApJ, 342, 1019
Mukadam, A. S., Montgomery, M. H., Winget, D. E., Kepler, S. O., & Clemens, J. C. 2006, ApJ, 640, 956
Mukadam, A. S., Owen, R., Mannery, E., et al. 2011, PASP, 123, 1423
Mukadam, A. S., Bischoff-Kim, A., Fraser, O., et al. 2013, ApJ, 771, 17
Mukadam, A. S., Pyrzas, S., Townsley, D. M., et al. 2015, in ASP Conf. Ser. 493, 19th European Workshop on White Dwarfs, ed. P. Dufour, P. Bergeron, & G. Fontaine (San Francisco, CA: ASP), 495
Mullally, F., Winget, D. E., Degennaro, S., et al. 2008, ApJ, 676, 573
Nelemans, G. 2005, in ASP Conf. Ser. 330, The Astrophysics of Cataclysmic Variables and Related Objects (San Francisco, CA: ASP), 27
Nogami, D., Hiroi, K., Suzuki, Y., et al. 2009, in ASP Conf. Ser. 404 ,The Eighth Pacific Rim Conf. on Stellar Astrophysics: A Tribute to Kam-Ching Leung, ed. S. J. Murphy, & M. S. Bessell (San Francisco, CA: ASP), 52
Norton, A. J., Butters, O. W., Parker, T. L., & Wynn, G. A. 2008, ApJ, 672, 524

Norton, A. J., Wynn, G. A., & Somerscales, R. V. 2004, ApJ, 614, 349
O'Donoghue, D., Kanaan, A., Kleinman, S. J., Krzesinski, J., & Pritchet, C. 2000, BaltA, 9, 375
Patterson, J., Thorstensen, J. R., Sheets, H. A., et al. 2011, PASP, 123, 130
Paxton, B., Bildsten, L., Dotter, A., et al. 2011, ApJS, 192, 3
Piersanti, L., Gagliardi, S., Iben, I. J., & Tornambé, A. 2003, ApJ, 583, 885
Senziani, F., Skinner, G., & Jean, P. 2008, ATel, 1372, 1
Shafter, A. W., & Macry, J. D. 1987, MNRAS, 228, 193
Sion, E. M. 1999, PASP, 111, 532
Szkody, P., Anderson, S. F., Brooks, K., et al. 2011, AJ, 142, 181
Szkody, P., Mukadam, A. S., Gänsicke, B. T., et al. 2013, ApJ, 775, 66
Taam, R. E., & Spruit, H. C. 1989, ApJ, 345, 972
Tody, D. 1993, in ASP Conf. Ser. 52, Astronomical Data Analysis Software and Systems II, ed. R. J. Hanisch, R. J. V. Brissenden, & J. Barnes (San Francisco, CA: ASP), 173
Townsley, D. M., & Bildsten, L. 2003, ApJL, 596, L227
Townsley, D. M., & Gänsicke, B. T. 2009, ApJ, 693, 1007
Wang, L., Baade, D., Höflich, P., et al. 2003, ApJ, 591, 1110
Warner, B. 1995, Cataclysmic variable stars (Cambridge: Cambridge Univ. Press)
Winget, D. E., Cochran, W. D., Endl, M., et al. 2003, in ASP Conf. Ser. 294: Scientific Frontiers in Research on Extrasolar Planets (San Francisco, CA: ASP), 59
Yoon, S.-C., & Langer, N. 2005, A&A, 435, 967